PHYSICAL REVIEW B **78**, 060405(R) (2008)

Dynamical coupling between ferromagnets due to spin transfer torque: Analytical calculations and numerical simulations

Sergei Urazhdin
Department of Physics, West Virginia University, Morgantown, West Virginia 26506, USA
(Received 18 May 2008; revised manuscript received 31 July 2008; published 18 August 2008)

We use a combination of analytical calculations and numerical simulations to demonstrate that electrical current flowing through a magnetic bilayer induces dynamical coupling between the layers. The coupling originates from the dependence of the spin transfer torque on the relative orientations of their magnetic moments. When the appropriate resonance conditions are satisfied, such coupling significantly modifies the behaviors of both layers, affecting the stability of the current-induced dynamical regimes and the efficiency of current-induced magnetic reversal.

DOI: 10.1103/PhysRevB.78.060405 PACS number(s): 75.60.Jk, 85.75.−d, 75.70.Cn

Current-induced spin transfer (ST) effect[1] is the most promising mechanism for manipulation of magnetic nanodevices due to the simplicity of the implementation and potential power benefits. The main obstacle for applications is the large magnitude of the current required for fast operation of devices. A basic magnetoelectronic device consists of a magnetic bilayer $F_1/N/F_2$, where F_1 is a magnet polarizing the current and F_2 is a nanomagnet whose configuration is changed by ST. Aside from the predicted anomalous dependence of current-induced dynamics on bias in tunnel junctions,[2] the effects of current are similar in tunnel junctions and spin valves. The following discussion is therefore pertinent to both metallic and insulating nonmagnetic spacers N. The main parameters characterizing the efficiency of spin transfer is the zero-temperature threshold current I_c for the onset of current-induced magnetic dynamics of F_2. For parallel (P) equilibrium configuration of the magnetic moments,[1,3]

$$I_c = eH_{\mathrm{eff}}S_2\alpha\gamma/g_2(0), \tag{1}$$

where e is the electron charge, S_2 is the total spin of F_2, H_{eff} is the effective magnetic field which includes magnetic anisotropy, α is the damping, γ is the gyromagnetic ratio, and $g_2(\theta_{12})$ is a function of the angle θ_{12} between the magnetic moments of F_1 and F_2, which depends predominantly on the spin-polarizing properties of F_1. Several directions have been pursued for reducing I_c such as enhancing the current polarization,[4] using two polarizing layers,[5] and decreasing H_{eff} by using devices with perpendicular anisotropy.[6] However, each of these methods only modestly contributes to ST efficiency and it now appears that their efficient combination will be needed to achieve the required performance.

Here, we discuss yet another mechanism affecting the efficiency of ST involving simultaneous current-induced excitation of both F_1 and F_2. We describe analytical results for a model system, neglecting the anisotropy of the ferromagnets, and present numerical calculations in macrospin approximation that take realistic magnetic anisotropies into account. Both calculations show that coupling due to ST can increase or decrease I_c with respect to the value given in Eq. (1), depending on the polarizing properties of F_1 and F_2.

Analytical model. We consider a model system of two single-domain magnets F_1 and F_2 represented by the unit vectors $\mathbf{s}_1$ and $\mathbf{s}_2$ in the direction of the magnetic moments. This model neglects the important effects of demagnetizing fields, dipolar coupling, and dynamical inhomogeneities but provides a physical insight into the coupling mechanism. The dynamics of the magnetic moments in the presence of current $I>0$ flowing from F_1 to F_2 is described by two Landau-Lifshitz equations coupled by the spin transfer torque (STT) term[1]

$$\frac{d\mathbf{s}_{1,2}}{dt} = \mathbf{s}_{1,2}\times\left[\gamma(\mathbf{H}-\alpha\mathbf{s}_{1,2}\times\mathbf{H}) + \frac{Ig_{1,2}}{eS_{1,2}}\mathbf{s}_1\times\mathbf{s}_2\right], \tag{2}$$

where $S_{1,2}$ are the spins of F_1, F_2. For simplicity, we assume the same α for both magnets and neglect the dependence of $g_{1,2}$ on the relative orientations of $\mathbf{s}_1$ and $\mathbf{s}_2$. In the limit $S_1 \gg S_2$, the last term in Eq. (2) for the dynamics of $\mathbf{s}_1$ is negligible due to the large value of S_1, resulting in a static solution for $\mathbf{s}_1$. Equation (2) then yields precession of $\mathbf{s}_2$ at a current I_{c0} given by Eq. (1), consistent with the models for single-magnet dynamics.

We are interested in the solution of Eq. (2) for comparable S_1 and S_2. We denote the azimuthal angle characterizing precession phase by ϕ and the polar angle characterizing precession amplitude by θ. Assume that STT induces simultaneous precession of S_1, S_2 around the magnetic field $\mathbf{H}$ with amplitudes θ_1 and θ_2. To demonstrate that the stable configuration involves precession of both magnets with the same phase, we assume that $\mathbf{s}_1$ lags behind $\mathbf{s}_2$ by a small angle $\Delta\phi$. The torque τ_1^{STT} exerted on $\mathbf{s}_1$ then acquires an additional azimuthal component, resulting in an increase in its angular frequency by $\Delta\omega_1 = \gamma I g_1 \sin(\theta_2)\sin(\Delta\phi)/[eS_1\sin(\theta_1)]$. Similarly, the azimuthal component of STT acting on $\mathbf{s}_2$ increases its frequency by $\Delta\omega_2 = \gamma I g_2 \sin(\theta_1)\sin(\Delta\phi)/[eS_2\sin(\theta_2)]$. The stability of in-phase precession requires that $\Delta\omega_1 > \Delta\omega_2$, which is satisfied if $[\sin(\theta_1)/\sin(\theta_2)]^2 < S_2/S_1$, as demonstrated below.

The stationary form of Eq. (2) for in-phase precession is

$$Ig_1\sin(\theta_2-\theta_1) = eS_1\alpha H\sin(\theta_1)$$

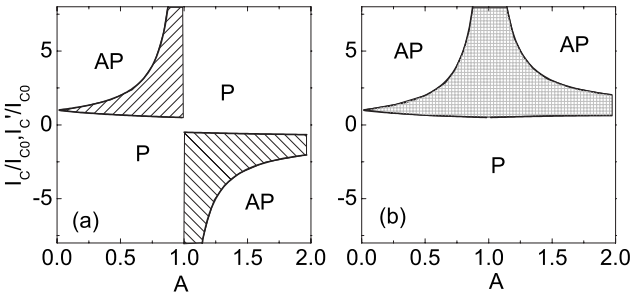

FIG. 1. Stability diagram for the analytical model of two-layer system with varied $A=S_1/S_2$. (a) $g_1=g_2$, bistable regions are hatched. (b) $g_1=-g_2$, the region of stable precession is filled. For $A<1$, I_{c0} is defined by Eq. (1). For $A>1$, I_{c0} is defined by Eq. (1) with S_2 replaced by S_1 to emphasize the dominance of this layer's dynamics.

$$Ig_2 \sin(\theta_2 - \theta_1) = eS_2 \alpha H \sin(\theta_2). \tag{3}$$

The spin-filtering properties of F_1 and F_2 are often similar, resulting in $g_1 \approx g_2$. Equation (3) then leads to

$$S_1 \sin(\theta_1) = S_2 \sin(\theta_2), \tag{4}$$

which satisfies the above condition for the stability of in-phase precession. Equation (3) yields the onset current for the precession $I_c=I_{c0}/(1-S_2/S_1)$. This expression is actually symmetric with respect to S_1 and S_2 [see Eq. (1)] and is thus valid regardless of their values.

The relation between the precession amplitudes is determined by the ratio $A=S_2/S_1$. In particular, the dynamics of $\mathbf{s}_1$ is negligible at $A \ll 1$. Precession of $\mathbf{s}_2$ can then occur only at $I=I_c>0$. Conversely, the dynamics of $\mathbf{s}_2$ is negligible at $A \gg 1$, while precession of $\mathbf{s}_1$ can occur at $I<0$. We also note that I_c diverges when the magnetic moments become equal $(A=1)$.

To determine the stability regimes of coupled precession, we insert Eq. (4) into the second of Eq. (3) giving

$$I = \frac{I_{c0}/A}{\sqrt{1/A^2 - 1 + \cos^2(\theta_2)} - \cos(\theta_2)}, \tag{5}$$

where $I_{c0}=\alpha\gamma HeS_2/g_2$. Equation (5) describes a monotonically *decreasing* function of θ_2, which implies that precession is unstable at any I. On the other hand, both $\theta_2=0$ and $\theta_2=\pi$ are stable in the range $I_c'=\frac{P}{1+A}<I<\frac{P}{1-A}=I_c$, where I_c' is the current at which the antiparallel (AP) state becomes stable. The resulting stability diagram is shown in Fig. 1(a), where the bistable regions are hatched.

As a consequence of the dynamical coupling due to STT, the value of I_c' is reduced by a factor of 2 at $A=1$ while I_c diverges. The current-induced bistability in devices with $A \approx 1$ should generally result in telegraph-type noise due to thermally activated transitions between the two stable configurations. Such noise is detrimental to most applications. However, such configuration may be useful if small-amplitude current-induced dynamics is undesirable. For $A<1$, dynamical coupling also makes it impossible to induce dynamical states at $I<0$. Similarly, dynamics cannot be induced at $I>0$ for $A>1$. This result also holds in more realistic calculations described below. The observation of bipolar current-induced excitations in symmetric nanopillars[7–9] indicates a significant inhomogeneity of current-induced dynamics in those experiments.

Applications of magnetoelectronic devices in microwave generation require I_c to be minimized and stable precession to be achieved over a significant range of I. We demonstrate below that I_c can be reduced by the current-induced coupling when g_1 and g_2 have opposite signs. This requires reversing the spin anisotropy of one of the ferromagnets. In metallic structures, this can be accomplished by doping F_1 or F_2 with impurities providing appropriate spin-dependent scattering in their bulk and/or by choosing N that inverts the spin anisotropy of electron scattering at F/N interface.[10] For simplicity, we now assume that $g_1=-g_2<0$. The torques exerted on the two moments now result in their mutual attraction at $I<0$, producing a stable collinear configuration for any A. Dynamical states are induced only by $I>0$ regardless of the value of A. The relative precession phases of $\mathbf{s}_1$ and $\mathbf{s}_2$ are now shifted by 180°. Estimates similar to the ones given above for $g_1, g_2>0$ show that this precessional configuration is stable. Equation (4) for the precession amplitudes of the two moments still holds but Eq. (5) is replaced with

$$I = \frac{I_{c0}/A}{\sqrt{1/A^2 - 1 + \cos^2(\theta_2)} + \cos(\theta_2)}. \tag{6}$$

The resulting stability diagram shown in Fig. 1(b) includes a region of stable coupled precession of the two magnets. At $A=1$, the precession onset current is reduced by a factor of 2, while the largest value of I at which the precession remains stable diverges.

Numerical simulations. To determine the effects of demagnetizing fields and dipolar coupling, we solved Eq. (2) numerically using the geometry and the magnetic properties typical for ST devices, in which F_1 and F_2 are Permalloy layers with thicknesses t_1 and t_2, patterned into an elliptical 120×60 nm^2 nanopillar. We used the material parameters known from the magnetotransport measurements.[11] Here, we describe the results of calculations taking into account only the demagnetizing fields calculated by approximating the magnetic layers with elongated ellipsoids. We neglect dipolar coupling to simplify the interpretation of current-induced behaviors and separately comment on its effects below.

We included the dependencies of the spin transfer efficiencies g_1, g_2 on the configuration of the magnetic system to take into account the slight experimental asymmetry between the $P \rightarrow AP$ and $AP \rightarrow P$ reversals.[4] The equations were numerically integrated by the stochastic Heun method with a time step of 2 ps. To verify the convergence, the step size was decreased by a factor of 2, which did not significantly affect the results. Random field approximation was used to model the thermal activation between different current-induced modes with temperature set to 50 K. The damping parameter $\alpha=0.03$ was used for both magnets.[12]

The model was tested for three limiting cases: $t_1 \gg t_2$, $t_1 \ll t_2$, and $t_1=t_2$. In the first case, STT induced the dynamics of only $\mathbf{s}_2$ and only at $I>0$. Figure 2(a) shows the normalized spectra of the component of $\mathbf{s}_2$ along the hard in-plane

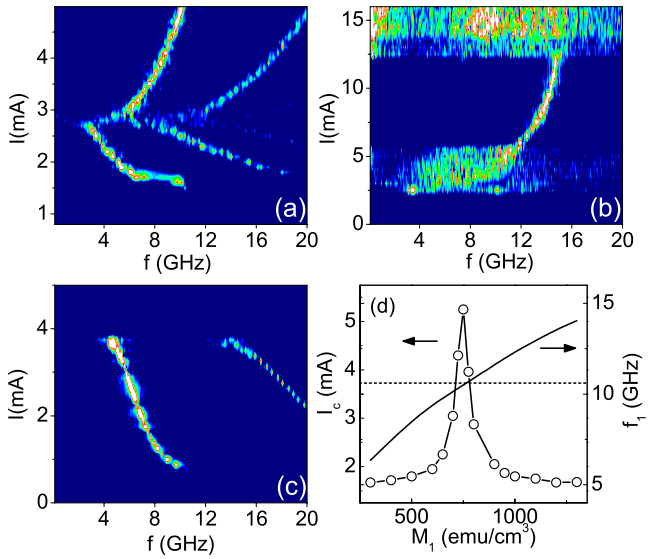

FIG. 2. (Color online) (a)–(c) Normalized spectral intensity for the dynamics of the in-plane hard-axis component of $\mathbf{s}_2$. (a) $A=0.2$, (b) $A=0.67$, (c) $A=1$, and $g_1=-g_2$. Lighter colors correspond to higher intensity. The same scale is used in all three plots. (d) Resonant behaviors of dynamical coupling for fixed $t_2=4$ nm and $M_2=800$ emu/cm^3. Symbols connected by line: I_c vs M_1 at a fixed $A=0.67$. I_c was determined by the condition that in-plane precession angle exceeds 0.2° while ramping the current at a rate of 0.01 mA/ns. Solid curve: Small-angle precession frequency of F_1. Dashed horizontal line shows small-angle precession frequency of F_2. The calculations were performed at $H=1$ kOe along the nanopillar easy axis.

axis for $A=0.2$. This component is convenient for characterization of the dynamical states, but the resulting relative intensities of peaks are different from the experimentally measured signals caused by magnetoresistance. The peaks correspond to several harmonics of the precession. After the onset of small-angle precession at $I_c=1.67$ mA, the frequency of precession decreases due to transition to large-angle clamshell precession trajectory. The transition to the out-of-plane precession at $I>2.6$ mA results in the increase in precession frequency. These results are consistent with the published calculations for single-layer dynamics[13] and are in overall agreement with the experiments.[14] Similar spectra were obtained for the dynamics of $\mathbf{s}_1$ at $I<0$ for $t_1 \ll t_2$. Calculations for $t_1=t_2$ yielded identical spectra for $\mathbf{s}_1$ and $\mathbf{s}_2$ regardless of the sign of I as expected for this symmetric geometry. Additionally, the calculations for $t_1=t_2$ and $H=0$ reproduced the sequential thermally activated flipping of $\mathbf{s}_1$ and $\mathbf{s}_2$ observed in symmetric magnetic nanopillars.[9]

The effects of dynamical coupling are illustrated in Fig. 2(b) for $A=0.67$. The onset current for the magnetic dynamics is larger than in Fig. 2(a) as expected from the analytical model. At $2.9<I<6$ mA, the data exhibit a broad excitation spectrum due to random transitions between clamshell-type and the out-of-plane precession of $\mathbf{s}_2$. These transitions are driven by the variations of the relative phase with the elliptical precession of $\mathbf{s}_1$, which is not phase coherent with $\mathbf{s}_2$. The formation of a sharp peak at $6<I<12$ mA is associated with the complete transition to out-of-plane precession of $\mathbf{s}_2$, resulting in nearly static deflection of $\mathbf{s}_1$ toward $\mathbf{s}_2$. At $I>12$ mA, the oscillations of $\mathbf{s}_1$ become sufficiently large to disrupt the periodic precession of $\mathbf{s}_2$, resulting in increasingly chaotic dynamics of both. The chaotic behaviors persisted in deterministic simulations at $T=0$, eliminating thermal fluctuations as their cause. Such behaviors are characteristic of multidimensional nonlinear dynamical systems.

At $A>0.67$, the broad excitation band at small I and the out-of-plane precession peak gradually disappeared. At $A=1$, only the $I>12$ mA continuum remained and similar features appeared at $I<-12$ mA. There were no excitations at $I<0$ for all $A<1$, in agreement with the analytical results. These results seem to be inconsistent with the intuitive picture according to which $I>0$ can induce the dynamics of $\mathbf{s}_2$ while $I<0$ can induce the dynamics of $\mathbf{s}_1$ even for $A<1$.[15] However, analysis of the magnetic trajectories shows that all oscillations of $\mathbf{s}_1$ at $I<0$ are efficiently suppressed by $\mathbf{s}_2$ closely following $\mathbf{s}_1$, reducing STT exerted on both layers.

Calculations for $g_1=-g_2$ showed a reduction in I_c as illustrated in Fig. 2(c) for $A=1$. The value $I_c=0.75$ mA $\approx I_{c0}/2$ is consistent with the results of the analytical model. The spectra do not exhibit broadening and chaotic dynamic characteristic of the calculations for $g_1=g_2$. The peaks in Fig. 2(c) abruptly terminate at $I=3.8$ mA due to the formation of a static stable configuration with $\mathbf{s}_1$ and $\mathbf{s}_2$ oriented opposite to each other perpendicular to the film plane. Such static configuration seems to be specific to $A=1$. It was not present in calculations for $A<1$.

The coupling depends on the dynamical properties of the ferromagnets. Figure 2(d) illustrates that for a fixed $A=0.67$, and M_1 varied between 300 and 1400 Oe, the small-angle precession frequency f_1 of F_1 varied between 6 and 14 GHz. I_c reached 5.25 mA at $M_1=760$ Oe, when the precession frequencies coincided. The full width at half maximum (FWHM) for the peak was 80 emu/cm^3, which corresponds to the difference of ± 0.3 GHz between the small-angle precession frequencies. It is interesting to note that the calculation in Fig. 2(b) was slightly off resonance, resulting in $I_c<5.25$ mA. However, the excitation became coherent at $I>5.25$ mA.

The dependence of the coupling efficiency on the parameters of the magnetic layers can be also estimated analytically for small-angle precession. In the coordinate system defined by x in the film plane along $\mathbf{H}$ and the nanopillar easy axis, y along the in-plane hard axis, and z perpendicular to the film plane, Eq. (2) for $\mathbf{s}_2$ yields

$$ds_{2y}/dt = \gamma s_{2z}(H+4\pi M_2) - \alpha\gamma s_{2y}(H+H_a) + Ig_2(s_{2y}-s_{1y})/eS_2, \quad (7)$$

$$ds_{2z}/dt = -\gamma s_{2y}(H+H_a) - \alpha\gamma s_{2z}(H+4\pi M_2) + Ig_2(s_{2z}-s_{1z})/eS_2, \quad (8)$$

where H_a is the in-plane anisotropy field and $4\pi M_2 \gg H, H_a$ was assumed. Similar equations can be written for $\mathbf{s}_1$. These equations can be solved by assuming that: (i) small-angle precession frequencies of the two magnets are similar and (ii) the last two terms are significantly smaller than the first term on the right and can therefore be averaged

over the precession cycle. In a steady state, the approximate solution has the form

$$s_{2y} = C\cos(\omega t), \tag{9}$$

$$s_{2z} = -C\sqrt{(H+H_{a2})/(H+4\pi M_2)}\sin(\omega t), \tag{10}$$

$$s_{1y} = AC\cos(\omega t+\delta), \tag{11}$$

$$s_{1z} = -AC\sqrt{(H+H_{a1})/(H+4\pi M_1)}\sin(\omega t+\delta). \tag{12}$$

Inserting these solutions into Eqs. (7) and (8) and the similar equations for $\mathbf{s}_1$ and requiring conservation of the adiabatic constants $s_{1y}^2+H+4\pi M_1/H+H_{a1}s_{1z}^2$ and $s_{2y}^2+H+4\pi M_2/H+H_{a2}s_{2z}^2$, we obtain $I_c=e\alpha\gamma(H+2\pi M)/g(1/S_1-1/S_2\cos\delta)$, $\Delta\omega\equiv\omega_2-\omega_1=I_c g\sin\delta(1/S_1-1/S_2)/e$. Here, $\omega_{1,2}=\gamma\sqrt{(H+H_{a1,2})(H+4\pi M_{1,2})}$ are the angular frequencies of uncoupled $\mathbf{s}_1$ and $\mathbf{s}_2$ and $|\Delta\omega|\ll\omega$ is assumed. To determine FWHM of the I_c vs $\Delta\omega$ curve, we treat δ in the first relation as a parameter implicitly dependent on $\Delta\omega$. I_c reaches its maximum value at $\delta=0$ and half of that at $\delta=\cos^{-1}(2-1/A)$ or $\delta\approx\pm 60°$ for $A=0.67$. The second relation then gives

$$2\Delta\omega(\delta=60°)=\sqrt{3}\alpha\gamma(H+2\pi M). \tag{13}$$

With the parameters used for calculations in Fig. 2, we obtain $2\Delta\omega=539\ \mathrm{s}^{-1}$ or $2\Delta f=340$ MHz in frequency units, in reasonable agreement with the numerical calculations [Fig. 2(d)]. With the exception of g_2, Eq. (13) depends on the same essential parameters as I_c in Eq. (1). In particular, small damping α results in a small I_c and therefore a narrow region of ST-induced coupling between F_1 and F_2. However, current-induced precession is highly nonlinear with respect to I. Therefore, at least some of the dynamical regimes of the magnetic bilayer are generally expected to be significantly affected by coupling, regardless of the difference between their small-angle precession frequencies.

It may be challenging to observe some of the calculated behaviors because of the additional effects of dipolar coupling and dynamical inhomogeneities, bringing the dynamics of the two magnets out of resonance. We have performed additional calculations to verify that dipolar coupling preserves the increase in the critical current and the spectral broadening in symmetric bilayers with similar polarizing properties, as well as the decrease in critical current in bilayers with opposite polarizing properties. The effects of inhomogeneous current-induced states are presently not fully understood even for single-layer dynamics. Therefore, we leave the analysis of their effects on the dynamical coupling to future studies. However, we point out that the dynamics near the excitation threshold is usually well described by the macrospin approximation.[16] Thus, we expect our macrospin model to be adequate at least in this regime.

This work was supported by the NSF under Grant No. DMR-0747609 and a Cottrell Scholar Award from the Research Corporation. I thank Lidia Novozhilova for help with numerical simulations.

[1] J. Slonczewski, J. Magn. Magn. Mater. **159**, L1 (1996).
[2] I. Theodonis, N. Kioussis, A. Kalitsov, M. Chshiev, and W. H. Butler, Phys. Rev. Lett. **97**, 237205 (2006).
[3] J. A. Katine, F. J. Albert, R. A. Buhrman, E. B. Myers, and D. C. Ralph, Phys. Rev. Lett. **84**, 3149 (2000).
[4] S. Urazhdin, N. O. Birge, W. P. Pratt, Jr., and J. Bass, Appl. Phys. Lett. **84**, 1516 (2004).
[5] G. D. Fuchs, I. N. Krivorotov, P. M. Braganca, N. C. Emley, A. G. F. Garcia, D. C. Ralph, and R. A. Buhrman, Appl. Phys. Lett. **86**, 152509 (2005).
[6] S. Mangin, D. Ravelosna, J. A. Katine, M. J. Carey, B. D. Terris, and E. E. Fullerton, Nature (London) **5**, 210 (2006).
[7] S. I. Kiselev, J. C. Sankey, I. N. Krivorotov, N. C. Emley, A. G. F. Garcia, R. A. Buhrman, and D. C. Ralph, Phys. Rev. B **72**, 064430 (2005).
[8] B. Ozyilmaz, A. D. Kent, M. J. Rooks, and J. Z. Sun, Phys. Rev. B **71**, 140403 (2005).
[9] W. Lim, N. Anthony, A. Higgins, and S. Urazhdin, Appl. Phys. Lett. **92**, 172501 (2008).
[10] M. AlHajDarwish, H. Kurt, S. Urazhdin, A. Fert, R. Loloee, W. P. Pratt, and J. Bass, Phys. Rev. Lett. **93**, 157203 (2004).
[11] J. Bass and W. P. Pratt, Jr., J. Phys.: Condens. Matter **19**, 183201 (2007).
[12] I. N. Krivorotov, N. C. Emley, J. C. Sankey, S. I. Kiselev, D. C. Ralph, and R. A. Buhrman, Science **307**, 228 (2005).
[13] S. I. Kiselev, J. C. Sankey, I. N. Krivorotov, N. C. Emley, R. J. Schoelkopf, R. A. Buhrman, and D. C. Ralph, Nature (London) **425**, 380 (2003).
[14] W.-L. Lim, A. Higgins, and S. Urazhdin, arXiv:0806.4731 (unpublished).
[15] M. Tsoi, J. Z. Sun, and S. S. P. Parkin, Phys. Rev. Lett. **93**, 036602 (2004).
[16] D. V. Berkov and J. Miltat, J. Magn. Magn. Mater. **320**, 1238 (2008).